Peer-reviewed version available at Energies 2017, 10, 1651; doi:10.3390/en10101651

Article

Novel supervisory control algorithm to improve the performance of a Real-time PV Power-Hardware-In-Loop simulator with non-RTDS

Dae-Jin Kim, Byungki Kim, Hee-Sang Ko, Moon-Seok Jang and Kyung-Sang Ryu*

System Convergence Laboratory, Korea Institute of Energy Research, Jeju, South Korea
djk@kier.re.kr, bk_kim@kier.re.kr, heesangko@kier.re.kr, msjang@kier.re.kr
* Correspondence: ksryu@kier.re.kr; Tel.: +82-64-800-2225

Abstract: A programmable DC power supply with Real-time Digital Simulator (RTDS)-based photovoltaic (PV) Power Hardware-In-the-Loop (PHIL) simulators have been used to improve the control algorithm and reliability of PV Inverter. This paper proposes a supervisory control algorithm for PV PHIL simulator with non-RTDS device that is an alternative solution of high cost PHIL simulator. However, when such a simulator with conventional algorithm which is used in RTDS is connected to a PV inverter, the output is in the transient state and it makes it impossible to evaluate the performance of the PV Inverter. Therefore proposed algorithm controls the voltage and current target values according to the constant voltage (CV) and constant current (CC) modes to overcome the limitation of the Computing Unit, DC power supply and also uses a multi-rate system to account for the characteristics of each component of simulator. A mathematical models of a PV system, programmable DC power supply, isolated DC measurement device and Computing Unit are integrated to form a real-time processing simulator. Performance tests using a PV PHIL simulator which is applied proposed algorithm connected a PV inverter are carried out and proved superiority and utility of this method against conventional methods.

Keywords: Photovoltaic; Power-Hardware-In-Loop-Simulator; Supervisory control algorithm; Real-time processing;

1. Introduction

Photovoltaic (PV) power generation is a technique of converting solar light into electricity. Since the French scientist Edmond Becquerel first discovered the photovoltaic effect in 1839, many advances have been realized for PV power generation, such as the reduced cost and improved efficiency and lifespan of solar cells. This is due to active research and development on the commercialization of solar cells after the oil shock in the 1970s. Because of recent environmental issues and the threat of climate change to the survival of mankind, PV power generation is playing a leading role to meeting the increasing demand for renewable energy. Not only is the distribution of utility-grade PV power plants to replace existing power plants increasing, but small-scale distributed power-grade PV power generators are also gaining prominence. Recently, advances have been made in electric vehicles (EVs) (various related studies have focused on EV charging stations connected to PV power generation), and the percentage of homes combining small PV and EVs that use it as an energy source has been increasing [1–8].

Research is being actively conducted not only on improving the performance of solar power itself (i.e., PV cells, modules, and arrays) but also on peripheral systems to use the generated power. In particular, various studies have been conducted on Maximum Power Point Tracking (MPPT) algorithms to control inverters, which are devices that convert the power generated from a PV, and maximize the output power of a PV system [9-13]. Tests can be performed to apply inverter control

algorithm to an actual PV system, but reproducibility is difficult because of changing environmental factors such as the temperature and irradiation. The high cost of implementing actual PV systems to study the improvement of the grid-tied or off-grid PV inverter performance is required in research and development efforts. In order to solve this problem, PV Power Hardware-In-the-Loop (PHIL) simulators, which can simulate and test PV arrays in Real-time, are being used to develop PV inverters [14-17]. PV PHIL simulators are generally composed of universal real-time digital simulator (RTDS) devices, but these are expensive owing to extra features, difficult to use owing to the expertise required to run the program, therefore generally, there is barrier to be widely used.

In this paper, a supervisory control algorithm for PV PHIL simulator with non-RTDS is proposed which can improve the output performance developed with a general Computing Unit connected to programmable DC power supply. A multi-rate system is applied to proposed algorithm considering the characteristics of each peripheral devices. A plant consisting of a mathematical model of PV system, control algorithm, calibrations is simulated using the MATLAB/SIMULINK and implemented a form of Real-time processing S/W by means of application program interface API to peripheral components, Real-time Work Shop (RTW), and MEX function. To validate the proposed control algorithm of PV PHIL simulator, an evaluation test is carried out. This included isolated measurement devices for the monitoring output of the DC power supply and digital signal processing of measured signals to interface with peripheral devices.

The paper is organized as follows: the next section explains the mathematical modeling of the PV system. Later, in Section 3, presents the proposed control algorithm of PV PHIL simulator against conventional control algorithm and Implementation works such as Real-time S/W, centralized control logic are presented in Section 4. Section 5 presents the simulation and test results validating the performance of the proposed algorithm. Finally, the conclusions close the paper.

2. Mathematical Properties of a PV System for the PHIL Simulator

2.1. Characteristics of PV Cells for the PHIL Simulator

PV cells are the basic components of PV systems. They can be classified by their manufacturing materials as silicon semiconductors or compound semiconductors. In most of the PV industry, PV cells are made of silicon semiconductors with p–n junctions. The mathematical models to predict the electrical properties of PV cells regarding irradiation and temperature are classified as ideal single-diode, practical single-diode, and two-diode. In this research, the practical single-diode model was used for the PV cell considering the simulator's real-time computing processing and dynamic model's accuracy. Figure 1 shows the equivalent circuit [18–20].

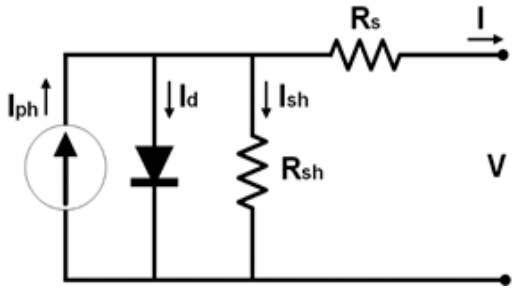

Figure 1. Equivalent circuit model of PV cell.

The output current of a PV cell can be generalized as shown in Equation (1) according to Kirchhoff's current law (KCL). Electrons and holes appear because of the photoelectric effect caused by light in the depletion layer of p–n semiconductors. The output current appears when a load is connected to both ends and follows the flow of electrons:

$$I = I_{ph} - I_d - I_{sh} \quad (1)$$

where I_{ph} is the photocurrent [A], I_d is the diode current [A], and I_{sh} is the current flowing in the shunt resistance [A].

The output current of this PV cell excludes the current flowing in the diode I_{ph}, and current flowing in the shunt resistance R_{sh}. The output current passes through R_s, and current I is finally output in from the PV cell. If arranged in order, I_d and I_{sh} are as shown in Equation (2):

$$I = I_{ph} - I_{sat}\left(e^{\frac{V+RI_s}{nV_t}} - 1\right) - \frac{V + IR_s}{R_{sh}} \quad (2)$$

where I is the PV cell output current [A], V is the PV cell output voltage [V], I_{sat} is the diode saturation current [A], n is the diode abnormal coefficient, R_s is the PV cell series resistance [Ω], and R_{sh} is the PV cell shunt resistance [Ω].

The diode thermal voltage, which is used to find the output current of Equation (2), is determined by the abnormal coefficient k value of the non-ideal diode model. This is considered in the following thermal voltage determination formula:

$$V_t = \frac{kT_{op}}{q} \quad (3)$$

where V_t is the diode thermal voltage [V], q is the electrical charge of the electron [C], k is the Boltzmann constant [J/K], and T is the operational temperature [K].

For a PHIL simulator to simulate a voltage-based output current model, Equation (4) is obtained when the PV cell current of Equation (2) is converted into the output voltage. I_{ph} and I_{sh} are dependent on the temperature and are necessary to solve Equation (4); they are determined according to the standard test conditions (STC), as shown in Equations (5) and (6). The bandgap energy E_0 varies depending on the type of semiconductor material and temperature. In this research, however, a constant value was used under the assumption of STC.

$$V = nV_t \ln\left[1 + \frac{I_{ph} - \frac{V}{R_{sh}} - I(1 + \frac{R_s}{R_{sh}})}{I_{sat}}\right] - IR_s \quad (4)$$

$$I_{ph} = \frac{G}{G_{STC}}\left[I_{ph\cdot STC} + \alpha(T_{op} - T_{STC})\right] \quad (5)$$

$$I_{sat} = I_{sat\cdot STC}\left(\frac{T_{op}}{nT_{op}}\right)^3 e^{\left[\frac{qE_g}{nT_{op}}\left(\frac{1}{T_{STC}} - \frac{1}{T_{op}}\right)\right]} \quad (6)$$

Here, G_{STC} is the irradiation under STC, T_{STC} is the temperature under STC, α is the temperature coefficient of the photon-induced current [%/C], and E_g is the bandgap energy of the semiconductor [eV].

2.2. Characteristics of PV Modules for the PHIL Simulator

PV modules are mostly composed of PV cells. The whole PV array is composed of a combination of serial and parallel PV modules depending on the design purpose. The operational voltage is determined by the numbers of serial and parallel PV modules (N_s, N_p). Shadows may appear depending on various environmental factors surrounding the installed PV array. Thus, the light

Preprints (www.preprints.org) | NOT PEER-REVIEWED | Posted: 22 September 2017 doi:10.20944/preprints201709.0109.v1

Peer-reviewed version available at Energies 2017, 10, 1651; doi:10.3390/en10101651

intensity on PV modules may not be the same, which can cause output mismatch inside the modules and lead to problems of deterioration and abrupt power generation decrease. To solve these problems, bypass diodes are used in serially connected PV modules, and blocking diodes are used in parallel PV modules, as shown in Figure 2.

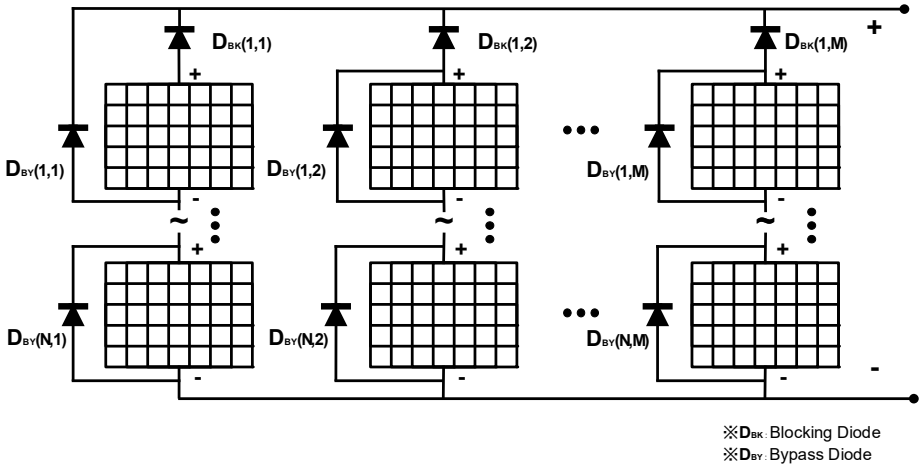

Figure 2. PV Array integrated with bypass and blocking diode.

The bypass diode is connected to the PV module in parallel. In the steady state where the light reaches the PV module homogeneously, the forward bias causes a reverse bias to the bypass diode, and no current flows. However, if an output mismatch between PV modules occurs due to shading, it becomes a reverse bias, which causes a forward bias to the bypass diode. This prevents damage caused by the hotspot phenomenon. The operating formula for the PHIL simulator can be expressed as follows:

$$V_{BY} = -\frac{n_{BY}kT_{op}}{q}\left[\frac{I - I_{ph}}{I_{satBY}} + 1\right] \quad (7)$$

where V_{BY} is the voltage drop caused by the bypass diode, n_{BY} is the bypass diode abnormal coefficient, and I_{satBY} is the bypass diode reverse saturation current.

The PV operating voltage in strings is defined by the number of serial and parallel modules (N_s,N_p) from Equation (4) and is expressed by the following voltage determination equation:

$$V = N_s n V_t \ln\left[1 + \frac{I_{ph} - \frac{V}{R_{sh}} - \frac{I}{N_p}\left(1 + \frac{R_s}{R_{sh}}\right)}{I_{sat}}\right] - \frac{I}{N_p}R_s \quad (8)$$

where N_s is the number of PV modules connected in series and N_p is the number of PV modules connected in parallel.

Regarding the parallel connection of PV modules, when a voltage imbalance occurs between modules in terms of strings, the output current can flow backwards into the low-voltage module with the shadow due to the voltage mismatch. To prevent this, a blocking diode is installed between modules, and a circuit is composed to prevent current from flowing into the PV module under normal conditions. The module voltage regarding the blocking diode operation can be generalized as follows:

$$V_{BK} = \frac{n_{BK}kT_{op}}{q}\left[\frac{I}{I_{sat}} + 1\right] \quad (9)$$

where V_{BK} is the voltage drop caused by the blocking diode and n_{BK} is the bypass diode abnormal coefficient.

Preprints (www.preprints.org) | NOT PEER-REVIEWED | Posted: 22 September 2017 doi:10.20944/preprints201709.0109.v1

Peer-reviewed version available at Energies 2017, 10, 1651; doi:10.3390/en10101651

The final output V_{out} of the PV array is the subtraction of the voltage drop V_{BK} used in the parallel connection from the maximum value between V and V_{BY}, which refer to the PV module output:

$$V_{out} = \max(V, V_{BY}) - V_{BK} \quad (10)$$

Based on the mathematical model of the PV array including the PV cell, MATLAB/Simulink is used to develop for simulation, as shown in Figure 3. The irradiation and temperature, which are external environment data, and the current value of the PV array are input to output the voltage and current [20].

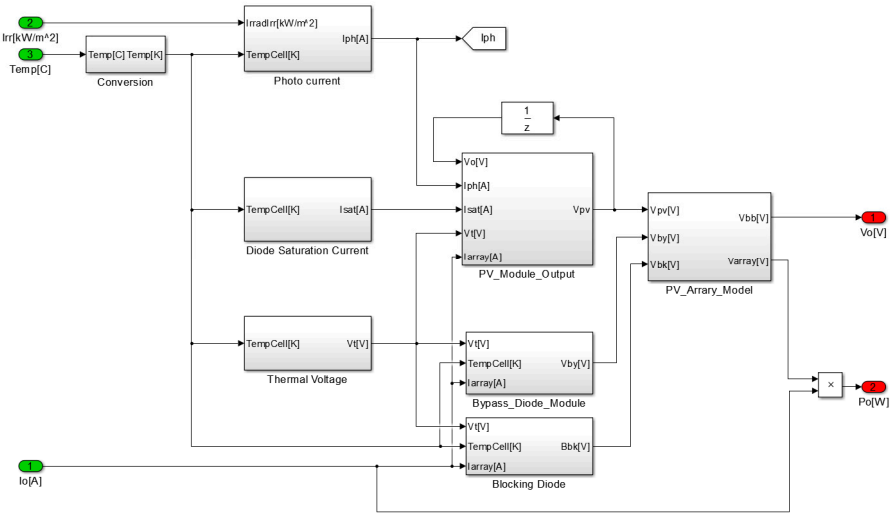

Figure 3. PV System array simulation model.

3. Advanced Operation Algorithm of a PV System for the PHIL Simulator

3.1. Conventional PV Simulator Operation Algorithm used in RTDS

In general, PV simulators that simulate the PV characteristics of invertors or load devices substitute the measured voltage and current values into PV mathematical models and transmit the obtained results to the DC power supply. Figure 4 shows the process of transmitting the generated voltage and current target values to the DC power supply after the input of the initial PV cell parameters PV_{Params}, irradiation $Ir(k)$, temperature $Te(k)$, measured voltage $V^m(k)$, and measured current $I^m(k)$ into the PV array model [14].

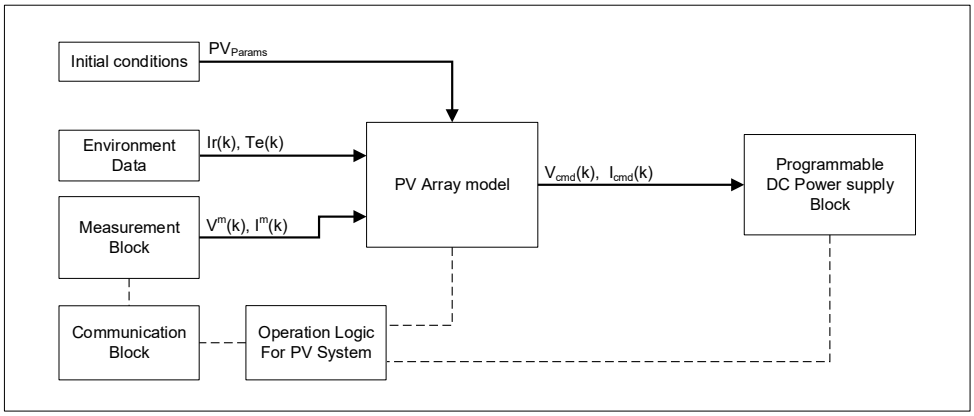

Figure 4. Conventional PV operation algorithm with RTDS.

Preprints (www.preprints.org) | NOT PEER-REVIEWED | Posted: 22 September 2017 doi:10.20944/preprints201709.0109.v1

Peer-reviewed version available at Energies 2017, 10, 1651; doi:10.3390/en10101651

However, the combination of general computing unit and typical programmable DC power supply has constraints such as sampling time to peripheral device, computing performance, and rectangular voltage and current output range which are divide into the constant voltage (CV) mode and constant current (CC) mode. One of these modes is activated depending on the load conditions. When a load is connected to the initial DC power supply, the CV mode is started; when the restricted current output range is exceeded, it changes to the CC mode to control the current. The CV mode is then no longer valid, and the output voltage cannot be controlled. Thus, when MPPT control is performed from an inverter, the constant voltage (CV) and constant current (CC) modes cross-operate, and the *I–V* curve of the actual PV system cannot be followed precisely owing to a transient output.

3.2. Proposed Supervisory Control Algorithm for the PV PHIL Simulator with non-RTDS

To improve the performance of PV PHIL simulator with non-RTDS connected to grid-tied PV inverter, a supervisory control algorithm and multi-rate system are proposed in this study to optimize the each component responsible for the main functions in Computing Unit, DC power supply, and isolated measurement device.

By external environment data to Computing Unit, the PV system characteristic values $V_{oc}(k)$ and $I_{sc}(k)$ are calculated from $F_{th}(Ir(k)$ and $T_e(k))$, as shown in Equations (11) and (12).

$$V_{oc} = N_s n V_t \ln\left[1 + \frac{I_{sc}}{I_{sat}}\right] \text{ for I} = 0 \tag{11}$$

$$I_{sc} = N_p\left[(I_{ph} - I_{sat}\left(e^{\frac{R_S R I_{sc}}{V_t}} - 1\right)\right] \text{ for V} = 0 \tag{12}$$

$V_b(k)$ and $I_b(k)$ are calculated from the function of $F_{Bias}(Ir, Te, V_{oc}, I_{sc})$. Finally, the PV array model results are considered along with $V_{mod}(k)$, and the reference value ($V_{cmd}(k)$, $I_{cmd}(k)$) that will be transmitted to the DC power supply is determined, as shown in Figure 5. The main blocks responsible for the DC power supply control, PV model, measurement devices, communication, and operation control are operated based on the multi-rate system as $S^1(k)$, $S^2(k)$, $S^3(k)$, $S^4(k)$, and $S^5(k)$, respectively.

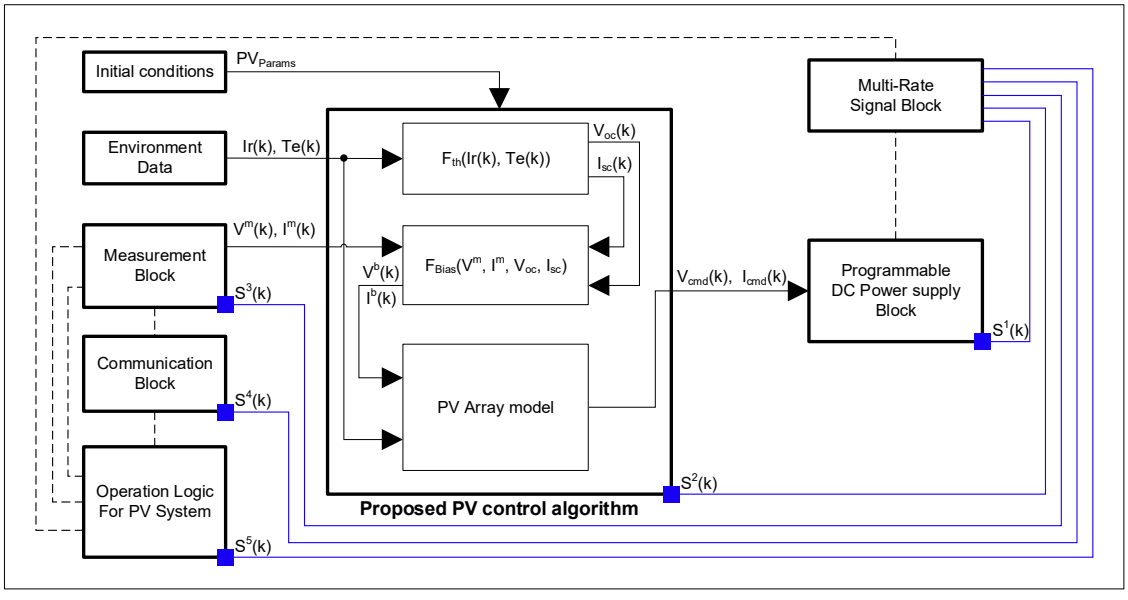

Figure 5. Proposed PV supervisory control algorithm with the multi-rate system.

Typical DC power supply start in CV mode, which controls the initial output voltage, and then change to CC mode, which controls the output current when the current limit is exceeded. In CC mode at DC power supply, the output voltage is not controllable due to activation only one mode at a time.

Preprints (www.preprints.org) | NOT PEER-REVIEWED | Posted: 22 September 2017 doi:10.20944/preprints201709.0109.v1

Peer-reviewed version available at Energies 2017, 10, 1651; doi:10.3390/en10101651

To overcome the limitations of such devices, the proposed control algorithm prevents transient states by comparing the voltage and current outputs in the DC power supply after calculating the I–V value with the maximum voltage V_{oc} and maximum current I_{sc} values according to the current input values of the environment variables. The environmental data $I_r(k)$ and $T_e(k)$ for the current step k and the PV system parameters are input, and Equations (11) and (12) are used to calculate the values of $V_{oc}(k)$ and $I_{sc}(k)$. After the DC power supply state are verified, the measurement voltage $V^m(k)$ and current $I^m(k)$ values being currently output are acquired from the isolated measurement device. The data are used to calculate $V_{mod}(k)$ and $I_{mod}(k)$ using the mathematical model of the PV module. The measured output current value and reference current value are compared, and the DC power supply mode is verified. Depending on the mode (CV or CC), the values and $min(A, B)$ functions calculated in the above step are used to output $V_{out}(k)$ and $I_{out}(k)$. $V_{cmd}(k)$ and $I_{cmd}(k)$ values can be found through rate limitation and saturation by considering the electrical properties of the PV system and peripheral devices and Figure 6 explains the algorithm in detail.

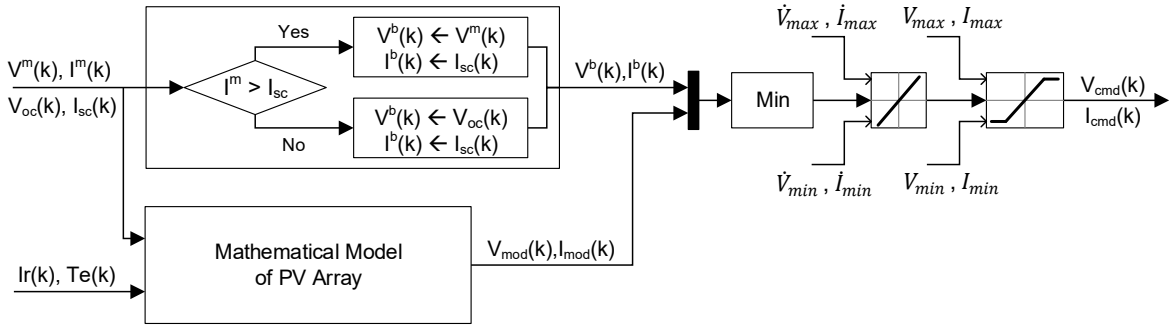

Figure 6. Proposed control algorithm with limitation values.

Because this PV PHIL simulator operates with multiple peripheral devices, it requires efficient control of the characteristics and states of each device. Thus, a multi-rate system that works in accordance with the current state of each device while considering the main control device load was developed. Table 1 presents the function blocks that operate each device and the load weight of each current state. Equation (13) is applied to the standard sample rate t_s, and the results of the operating cycle of each device (t_{DC}, t_{MC}, t_{MU}, and t_{CU}) are obtained. Finally, the above results are used to generate the operating signs of $S^{1–5}$ through the pulse generator function *PulGen*(), as shown in Equation (14). The cycle of the main block that works in connection with the peripheral devices operates at multiple rates of $S^1(k)$, $S^2(k)$, $S^3(k)$, $S^4(k)$, and $S^5(k)$. The DC power supply transmits and performs the final reference values of voltage $V_{cmd}(k)$ and current $I_{cmd}(k)$.

Table 1. Load weight of each major function block.

Function block	Initial stage (IS)	System test (ST)	Normal operation (NP)	Normal stop (NS)
DC power supply (DC)	w_{DC}^{IS}	w_{DC}^{ST}	w_{DC}^{NP}	w_{DC}^{NS}
Main computing unit (MC)	w_{MC}^{IS}	w_{MC}^{ST}	w_{MC}^{NP}	w_{MC}^{NS}
Measurement unit (MU)	w_{MU}^{IS}	w_{MU}^{ST}	w_{MU}^{NP}	w_{MU}^{NS}
Communication unit (CU)	w_{CU}^{IS}	w_{CU}^{ST}	w_{CU}^{NP}	w_{CU}^{NS}

Preprints (www.preprints.org) | NOT PEER-REVIEWED | Posted: 22 September 2017 doi:10.20944/preprints201709.0109.v1

Peer-reviewed version available at Energies 2017, 10, 1651; doi:10.3390/en10101651

$$t_{Function\ Block} = t_s \times \frac{w^{State}_{Function\ Block}}{4} \times \sum w^{State}_{Function\ Block}\ (w \geq 1) \quad (13)$$

$$[S^1\ S^2\ S^3\ S^4\ S^5]^T = PulGen(\ [t_{DC}\ t_{MC}\ t_{MU}\ t_{CU}\ t_{MC}]^T\ ) \quad (14)$$

4. Implementation of PV PHIL Simulator

4.1. Architecture of the Proposed PV PHIL Simulator

A proposed PV PHIL simulator with non-RTDS is composed of DC measurement that can verify the voltage and current values in connection with loads, programmable DC power supply, and Computing Unit which has core functions such as calculation of mathematical model of PV system, communication to peripheral devices, operation, and visualization, as shown in Figure 7. In this system, the Computing Unit and DC power supply interface transmit and receive data through USB communication, and the V–I output value calculated according to the irradiation and temperature data is sent depending on the DC power supply's current mode. In other words, the voltage and current values measured through serial communication with the analog circuit connected to the load are calibrated and utilized. EtherNET-based TCP/IP communication is performed with peripheral devices for real-time visualization and external environment data.

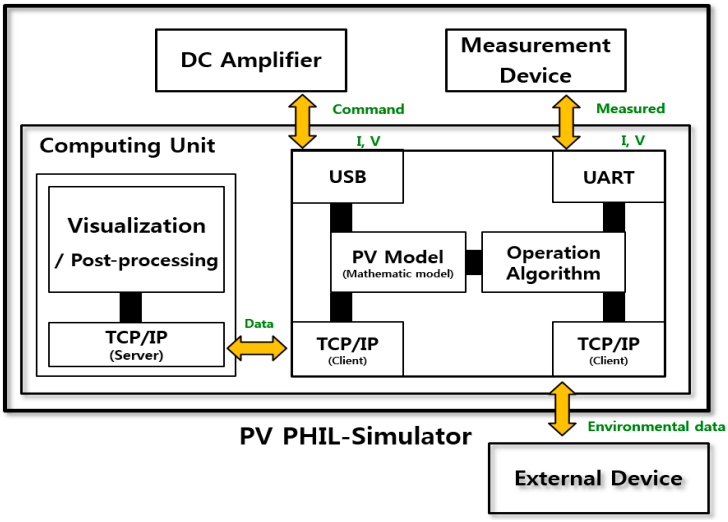

Figure 7. Architecture and data interface of the proposed PV PHIL.

4.2. Integration and conversion to Real-time processing

Due to the inputs and outputs are determined from current state of each component, it is necessary to operate PV PHIL simulator systematically. Therefore the centralized control logic is developed to perform the test with certain scenario and is shown in Figure 8, which is described in detail below.

Step 1. PV PHILS Initialization procedure: Check the system parameters, UART and TCP/IP communication check, Initialization to the Input and Output

Step 2. Pre-start up procedure: Initial stage to DC power supply and Enable the output power

Step 3. Check the state of each component: Communication check and current state of DC power supply, Isolated measurement device and other peripheral devices

Peer-reviewed version available at Energies 2017, 10, 1651; doi:10.3390/en10101651

Step 4. Data processing: Acquisition of the measurement data, calibration process and visualization to the GUI

Step 5. Supervisory control algorithm: Computing the mathematical model of PV system with environmental variables and measured data

Step 6. Execution process: Send the set values to DC power supply and check the fault

Step 7. Repeat the Step 3. ~ Step. 6 until the end of test

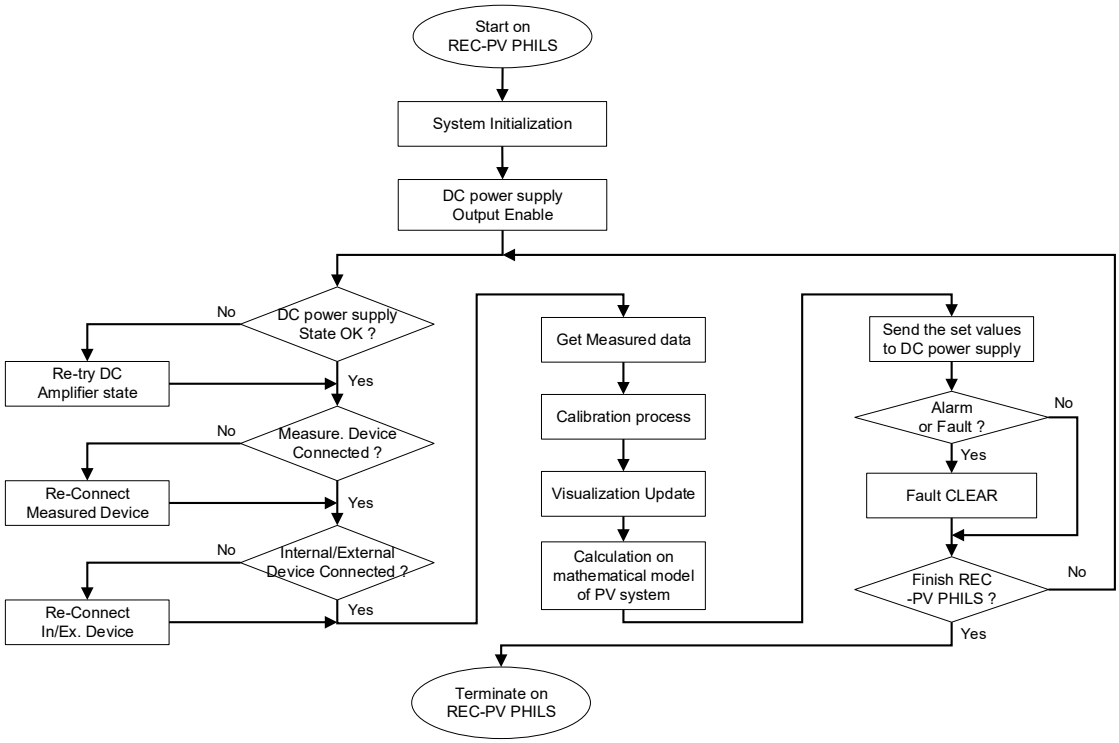

Figure 8. Centralized control logic of the proposed PV PHIL simulator.

On the other hand, the software elements including the mathematical model of the PV system mentioned in section 2 should be connected with the hardware and synchronous in Real-time using a general Computing Unit, rather than a special device equipped with an expensive RTDS. An application program interface (API) of programmable DC power supply, MATLAB, Real-time Workshop (RTW), and MEX function are used for code conversion and deployment to Real-time S/W, as shown in Figure 9.

Preprints (www.preprints.org) | NOT PEER-REVIEWED | Posted: 22 September 2017 doi:10.20944/preprints201709.0109.v1

Peer-reviewed version available at Energies 2017, 10, 1651; doi:10.3390/en10101651

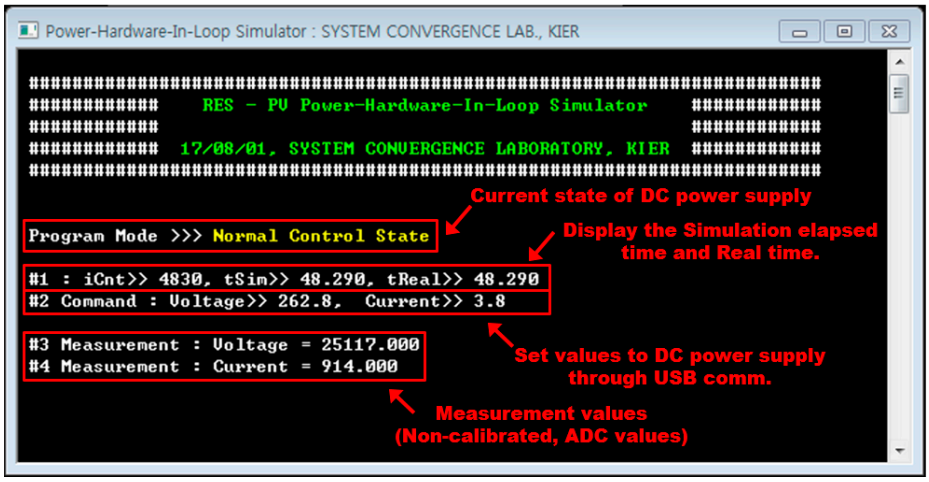

Figure 9. Real-time based PV PHIL Simulator S/W.

5. Performance Evaluation of the PV System for the PHIL Simulator

To validate the effectiveness of the proposed advanced PV control algorithm and the proposed simulator, an experiment was performed. The proposed method and a conventional method were compared using simulator equipment. The test results were used to compare and analyze the performance characteristics of both methods.

5.1. PV Array Simulation and Test Conditions

The performance of the proposed algorithm was evaluated with a commercial PV array [21] and Table 2 presents its parameters. The current–voltage characteristics graph of the PV array was calculated with the mathematical model under variable irradiation and temperature conditions and verified. A simulation was performed under two sets of conditions: the irradiation was fixed to 1000 W/m² while the temperature varied from 0 °C to 100 °C in 25 °C increments, and the temperature was fixed to 25 °C while the irradiation was increased from 200 W/m² to 1000 W/m² in 200 W/m² increments.

Table 2. Specifications of the PV array.

Category	Value	Unit
Model	MSX - 60	-
Cell type	Polycrystalline silicon	-
Maximum power (P_{max})	60	W
Voltage at P_{max} (V_{mp})	17.1	V
Current at P_{max} (Imp)	3.5	A
Open-circuit voltage (V_{oc})	21.1	V
Short-circuit current (I_{sc})	3.8	A
Diode quality factor	1.2	-
PV diode band-gap energy	1.124	eV
Number of series cells	36	-
Number of parallel cells	1	-
Number of parallel modules	12	-
Number of parallel modules	1	-

To compare and analyze the performances of the proposed algorithm and the conventional method for a PV PHIL simulator using a DC power supply, a 3 kW PV inverter connected to the system was used. The test was performed at 1000 W/m² and 25 °C. For the current–voltage graph

considering the PV array's irradiation and temperature, the operating point was defined with the MPPT control algorithm for the connected inverter. The PV PHILS operating characteristics and performance were compared and analyzed. Tables 3 and 4 present the detailed specifications of the DC power supply and inverter, respectively.

Table 3. Specifications of the programmable DC power supply.

Category	Value	Unit
Output rating voltage	0–315	V
Output rating current	0–8.4	A
Output power	2600	W
Programming accuracy	0.1% + 450.0 mV	-
Ripple and noise (20 Hz–20 MHz)	≤ 25 mVrms	-
AC input rating	Single phase 220 V ± 10% 50–60 Hz	-

Table 4. Specifications of the PV inverter.

Category	Value	Unit
Manufacturer	DASSTECH	-
Model	DSP-123K2	-
Max. DC power	3300	W
PV voltage range MPPT	110–450	V
Max. input current	15	A
Nominal AC output	3000	W
AC voltage output	220–240	V
AC connection	Single phase	-
Max. efficiency	96.7	%

5.2. Simulation Analysis of Performance Characteristics

To exactly implement the PV array characteristics according to the irradiation and temperature changes in the PV PHIL simulator, the current–voltage characteristics of the PV array were analyzed in MATLAB with variable external factor conditions. The PV array's mathematical model and real-time operable single-diode PV cell proposed in Section 2 were used. The current–voltage characteristics of the PV array were analyzed while the irradiation and temperature conditions were changed, and the typical current–voltage characteristics proposed by the manufacturer were compared to verify the degree of concordance and accuracy of the results. Figure 10 shows that the voltage–current characteristics of the PV array according to the mathematical model and the voltage and current levels at the maximum current follow-up point proposed by the manufacturer agreed when the temperature was set at 25 °C and the irradiation was incrementally increased from 200 W/m^2 to 1,000 W/m^2.

Preprints (www.preprints.org) | NOT PEER-REVIEWED | Posted: 22 September 2017 doi:10.20944/preprints201709.0109.v1

Peer-reviewed version available at Energies 2017, 10, 1651; doi:10.3390/en10101651

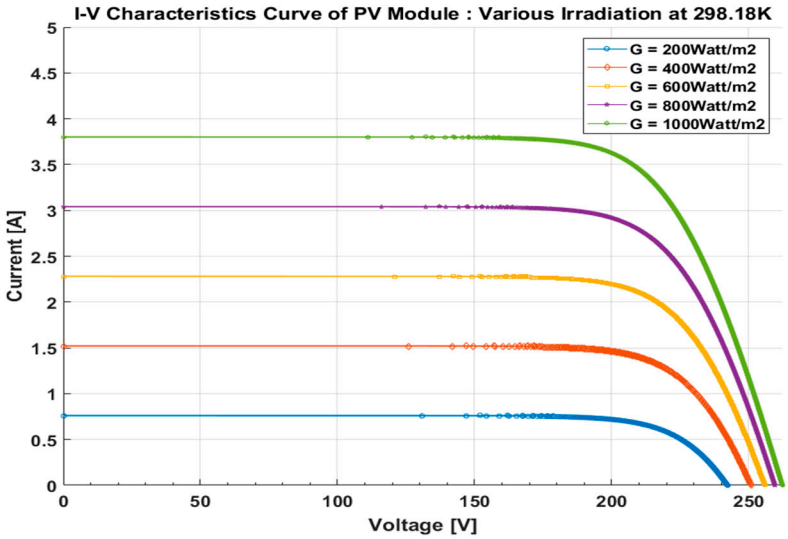

Figure 10. PV Array I-V Curve with various irradiation.

Figure 11 verifies that the voltage–current characteristics of the PV array according to the mathematical model and the voltage and current levels at the maximum current follow-up point proposed by the manufacturer matched when the irradiation was fixed at 1000 W/m² and the temperature was incrementally increased from 0 °C to 100 °C . Therefore, applying the proposed mathematical model to the PV-PHIL simulator was proven to provide the same characteristics as the operation of an actual PV system.

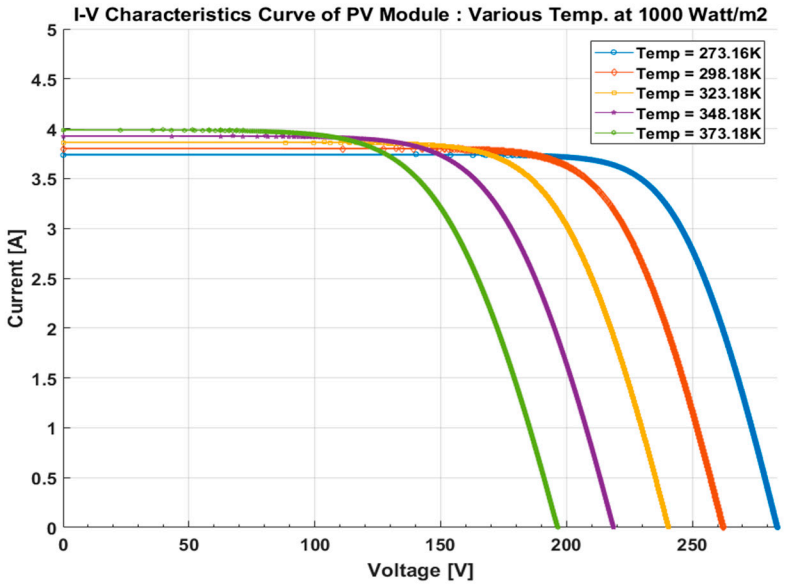

Figure 11. PV Array I-V Curve with various temperature.

5.3. Experiment Analysis of Performance Characteristics

To validate the accuracy of the proposed simulator, Real-time S/W which is included in the mathematical model described in Section 2, the PV control algorithm of the conventional method described in Section 3, and the centralized control logic described in Section 4 is applied to the PV-PHIL simulator to perform the tests with certain scenarios as shown in Figure 12.

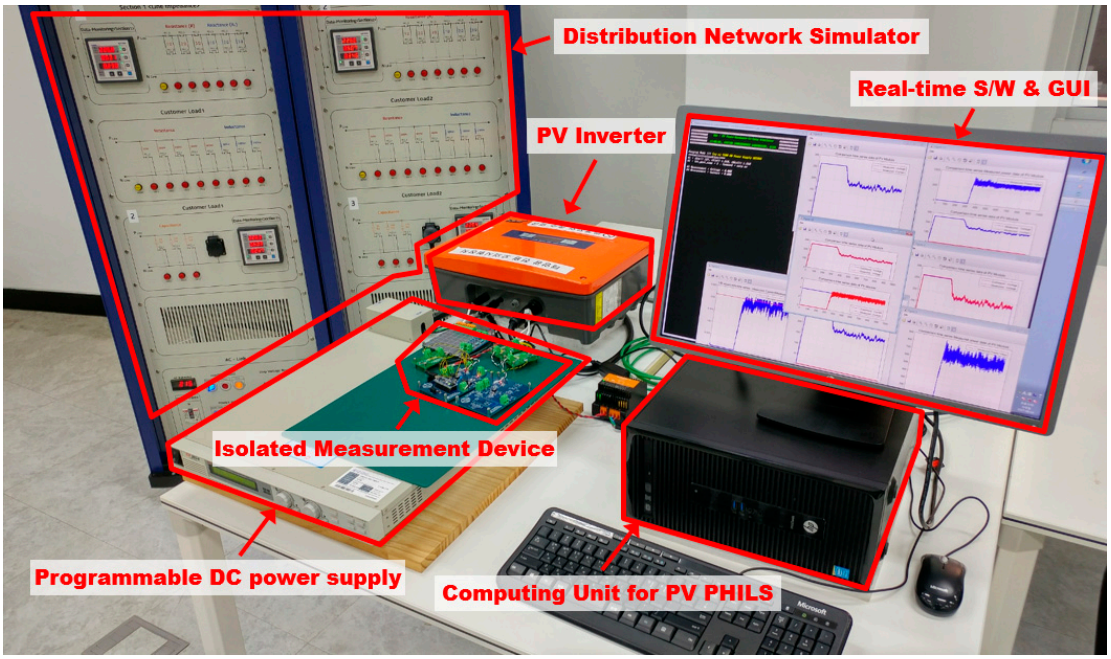

Figure 12. Experiment of PV PHIL Simulator with Grid-tied PV Inverter.

The initial environment conditions are an irradiation of 1000 W/m² and temperature of 25 °C. No shadow is assumed to appear on any PV module. As shown in Figure 13, with the conventional algorithm of the PV PHIL simulator, the PV array maintained the maximum output voltage V_{oc} state before being connected to the inverter system. However, after connection of the PV inverter to the grid, the voltage and current at the maximum power follow-up point varied continuously and irregularly.

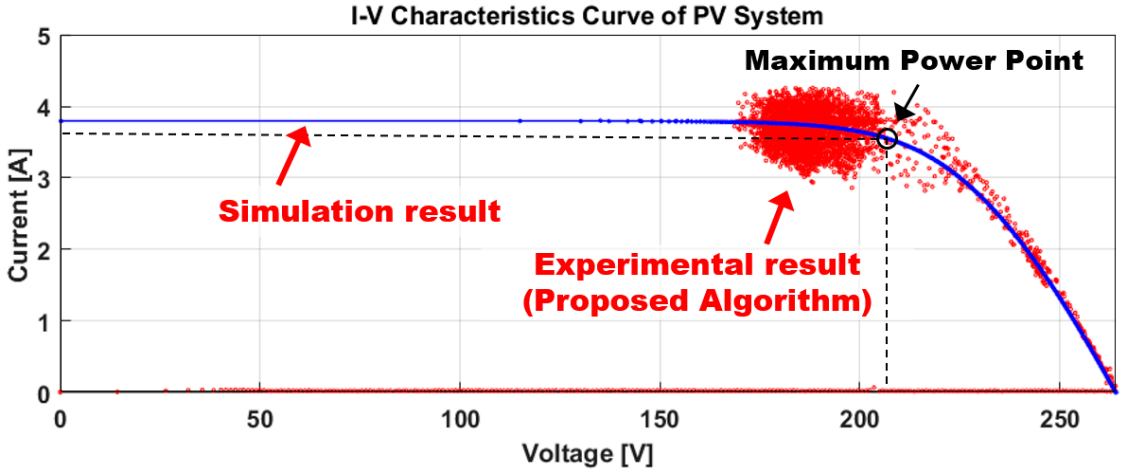

(a)

Preprints (www.preprints.org) | NOT PEER-REVIEWED | Posted: 22 September 2017 doi:10.20944/preprints201709.0109.v1

Peer-reviewed version available at Energies 2017, 10, 1651; doi:10.3390/en10101651

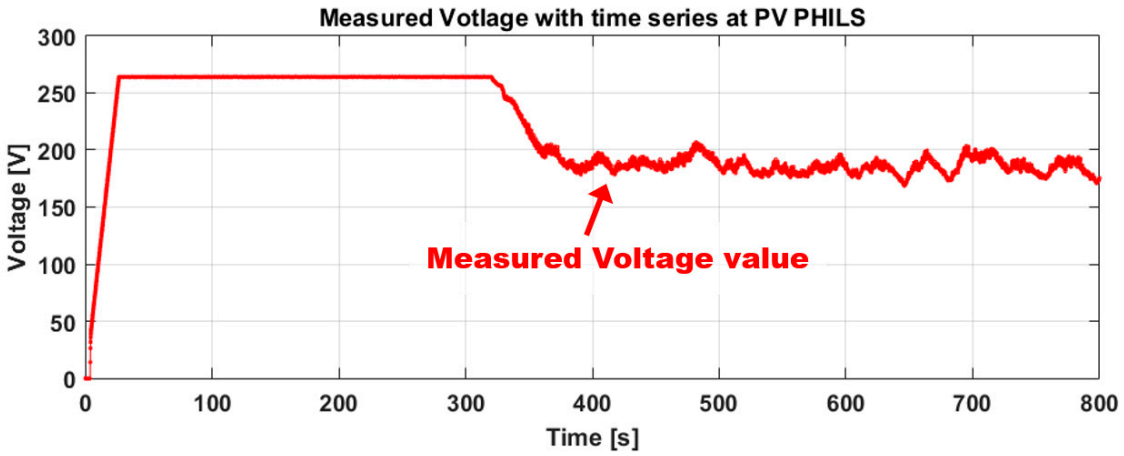

(b)

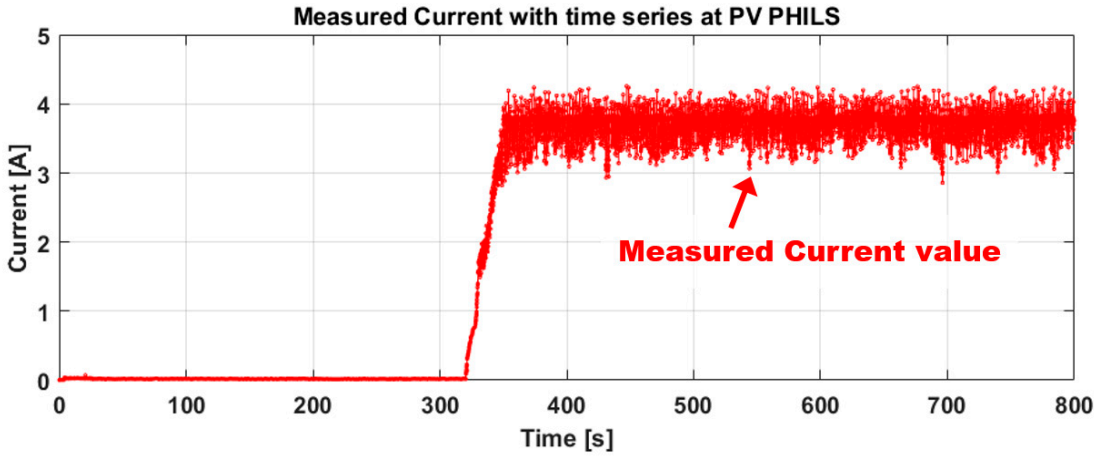

(c)

Figure 13. Experiment result with conventional operation algorithm of PV PHILS. (a) I-V Curve characteristic graph of PV System (b) DC power supply voltage output with time series (c) DC power supply current output with time series.

As the PV array output current approached I_{sc}, the I–V curve of the simulation was not followed, and the current–voltage output of the DC power supply was in the transient state. Therefore, in the inverter, the input power varied greatly over time, the MPPT control became unavailable, and the efficiency and performance decreased. In conclusion, when the performance of the PV inverter and MPPT algorithm was evaluated with the PV PHIL simulator using the conventional algorithm, the same characteristics as the actual PV could not be simulated, so a precise evaluation could not be performed.

When the proposed advanced operation algorithm was applied to the PV PHIL simulator under the same conditions described above, the initial output characteristics before connection to the PV inverter system revealed the same V_{oc} state as in the case of the conventional algorithm. After connection to the system, the maximum power point tracking was followed. The DC power supply's output current for the simulated PV array increased with the same pattern as the simulation described in the previous section, as shown in Figure 14. Therefore, with the proposed algorithm, the same characteristics as the actual PV were precisely simulated. Thus, the performance could be successfully evaluated.

Preprints (www.preprints.org) | NOT PEER-REVIEWED | Posted: 22 September 2017 doi:10.20944/preprints201709.0109.v1

Peer-reviewed version available at Energies 2017, 10, 1651; doi:10.3390/en10101651

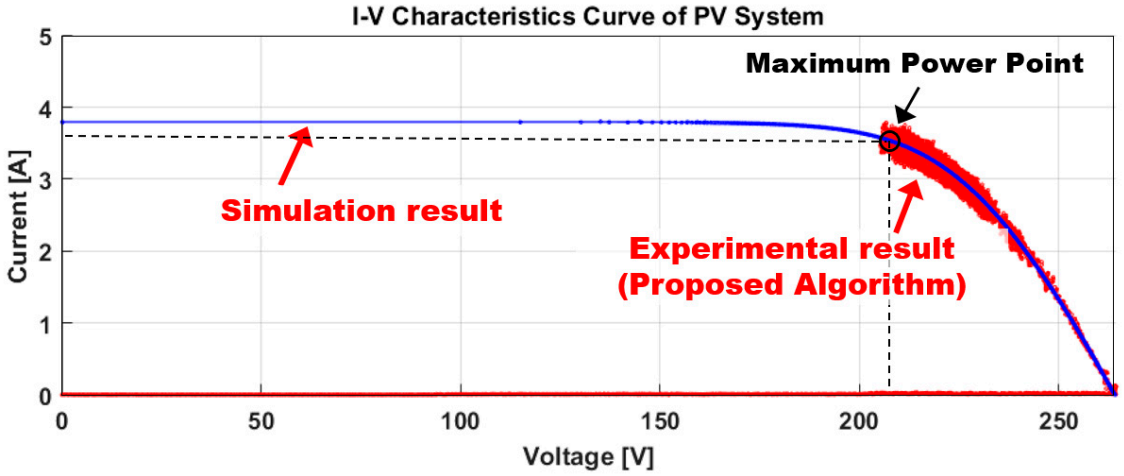

(a)

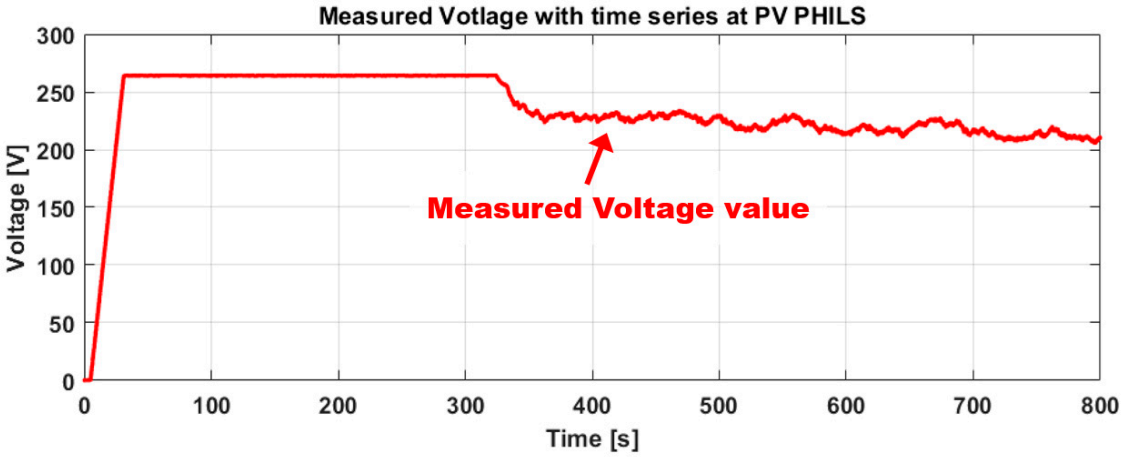

(b)

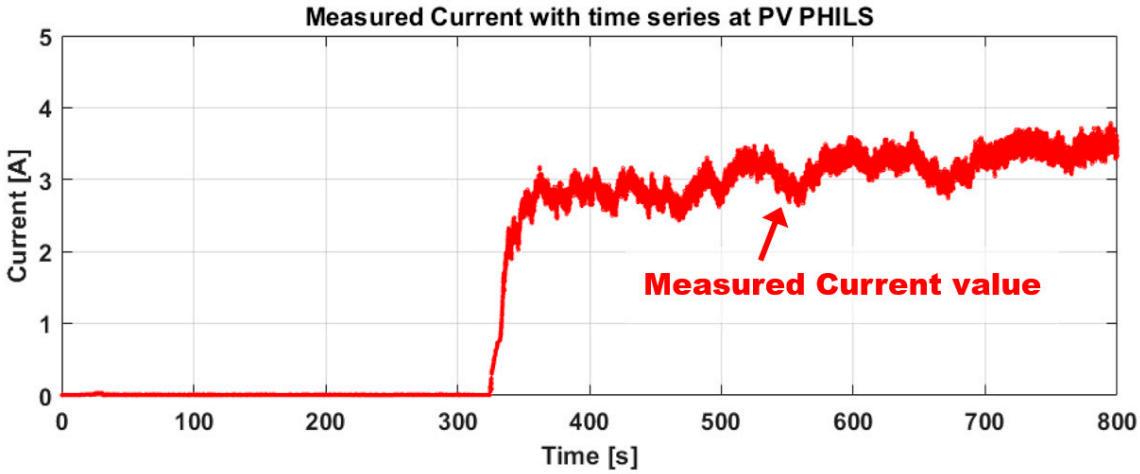

(c)

Figure 14. Experiment result with proposed advanced operation algorithm of PV PHILS. (a) I-V Curve characteristic graph of PV System (b) DC power supply voltage output with time series (c) DC power supply current output with time series.

Preprints (www.preprints.org) | NOT PEER-REVIEWED | Posted: 22 September 2017 doi:10.20944/preprints201709.0109.v1

Peer-reviewed version available at Energies 2017, 10, 1651; doi:10.3390/en10101651

To verify the performance of the PHILS algorithm, the Error Current is calculated by the results of each algorithm against the reference values performed through simulation as shown in Equation (15). Reference value of PV output current generated from PHILS is created by $LUT()$ function which has the Look-Up table of PV I-V Characteristic. Figure 15 shows the result of both algorithm and it is clear that the proposed algorithm has much better performance compared to conventional algorithm for PHIL simulator.

$$\text{Error Current(t)} = \sqrt{LUT(V^m(t)) - I^m(t)^2} \quad (15)$$

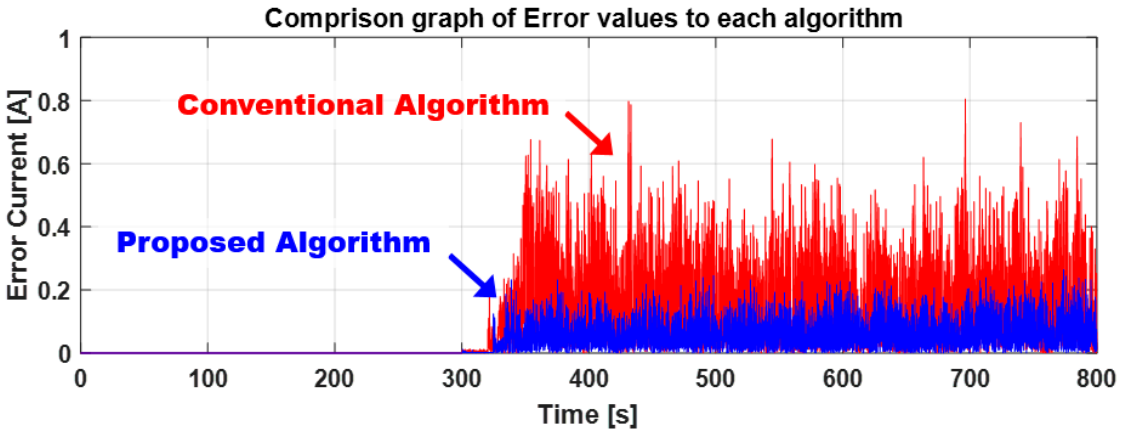

Figure 15. Error compared to reference value to each algorithm.

6. Conclusions

In this research, a supervisory control algorithm for PV PHIL simulators that use programmable DC power supply is proposed as a substitute for existing high-priced RTDS equipment. The effectiveness of this control algorithm was proven by comparison with conventional methods. The main results are summarized as follows.

(1) The conventional PV algorithm which is used in RTDS equipment was applied to the PV PHIL simulator proposed in this study, but the output is in transient state. However the proposed algorithm confirmed the stable output state with grid-tied PV inverter. In addition, grid-tied PV Inverter was able to perform MPPT control in PV PHIL simulator with the proposed algorithm.

(2) A Real-time operating program which is applied to the proposed algorithm, operating control logic, and API functions of peripheral devices was developed and verified the improved performance of the PV PHILS by means of general Computing Unit, DC power supply, and peripherals.

(3) With the spreading use of distributed PV power such as household PVs and modular PV containers for isolated areas, the PV PHIL simulator can be used to increase the performance, efficiency, and safety of PV inverters and thus increase competitiveness.

Acknowledgments:

This research was performed in 2017, funded by the Ministry of Trade, Industry and Energy, and supported by the Korean Energy Technology Evaluation and Planning (KETEP) (No. 20172410100030).

This work was conducted under the framework of Research and Development Program of the Korea Institute of Energy Research (KIER) (No. B7-2442).

Author Contributions: All of the authors contributed to publishing this paper. Dae-Jin Kim carried out modeling, simulations and compiled the manuscript. The literature review and experiments were performed by

Kung-Sang Ryu and Byungki Kim. Hee-Sang Ko and Moon-Seok Jang collected the data and investigated early works.

Conflicts of Interest: The authors declare no conflict of interest.

References

1. Hung, D.Q.; Dong, Z.Y.; Trinh, H. Determining the size of PHEV charging stations powered by commercial grid-integrated PV systems considering reactive power support. *Appl. Energy* **2016**, *183*, 160–169.
2. Ul-Haq, A.; Cecati, C.; Al-Ammar, E.A. Modeling of a Photovoltaic-Powered Electric Vehicle Charging Station with Vehicle-to-Grid Implementation. *Energies* **2017**, *10*, 4.
3. Khana, O.; Xiaob, W.; Review and qualitative analysis of submodule-level distributed power electronic solutions in PV power systems. *Renewable and Sustainable Energy Reviews* **2017**, *76*, 516–528
4. Zhang, Q.; Tezuka, T.; N. Ishihara, K.; C. Mclellan, B. Integration of PV power into future low-carbon smart electricity systems with EV and HP in Kansai Area, Japan. *Renewable Energy* **2012**, *44*, 99–108
5. Fathabadi,, H. Novel solar powered electric vehicle charging station with the capability of vehicle-to-grid. *Sol. Energy* **2017**, *142*, 136–143.
6. Locment, F.; Sechilariu, M.; Forgez, C. Electric Vehicle Charging System with PV Grid-connected Configuration. In Proceedings of the IEEE Vehicle Power and Propulsion Conference (VPPC), Lille, France, 1–3 September **2010**.
7. Birnie, D.P., III. Solar-to-Vehicle (S2V) Systems for Powering Commuters of the Future. J. *Power Sources* **2009**,186, 539–542.
8. Erickson, L.E.; Robinson, J.; Brase, G.; Cutsor, J. Solar Powered Charging Infrastructure for Electric Vehicles: A Sustainable Development; CRC Press: Boca Raton, FL, USA, **2016**.
9. Xiao, B.; Hang L.;Mei J.,Modular Cascaded H-Bridge Multilevel PV Inverter With Distributed MPPT for Grid-Connected Applications, *IEEE Transactions on Industry Applications* **2015**, 51(2), 1722-1731.
10. Moon, S.; Yoon, S.G.; Park, J.H., A New Low-Cost Centralized MPPT Controller System for Multiply Distributed Photovoltaic Power Conditioning Modules, *IEEE Transactions on Smart Grid* **2015**, 6(6) 2649 – 2658.
11. Karbakhsh, F.; Amiri, M.; Zarchi, H.A., Two-switch flyback inverter employing a current sensorless MPPT and scalar control for low cost solar powered pumps, *IET Renewable Power Generation* **2017**, 11(5), 669-677
12. Wang, Y.; Yu, X., Comparison study of MPPT control strategies for double-stage PV grid-connected inverter, Industrial Electronics Society, IECON 2013 - 39th Annual Conference of the IEEE, Vienna, Austria, Nov. 10-13 **2013**, 1561 - 1565.
13. Rout, A.; Samantara, S.; Dash, G. K., Modeling and simulation of hybrid MPPT based standalone PV system with upgraded multilevel inverter, India Conference (INDICON), 2014 Annual IEEE, Pune, India, Dec. 11-13 **2014**, 1-6.
14. Nzimako, O.; Wierckx, R., Modeling and Simulation of a Grid-Integrated Photovoltaic System Using a Real-Time Digital Simulator. *IEEE Trans. Ind. Applications.* **2016**, *53*(2), 1326–1336.
15. Khazaei, J.; Piyasinghe, L.; Miao, Z., Real-time digital simulation modeling of single-phase PV in RT-LAB, PES General Meeting | Conference & Exposition, National Harbor, MD, USA 2014 IEEE, 27-31 July 2014, 1-5.
16. Mai, X. H.; Kwak, S.K.; Jung, J.H., Comprehensive Electric-Thermal Photovoltaic Modeling for Power-Hardware-in-the-Loop Simulation (PHILS) Applications. *IEEE Trans. Ind. Electronics.* **2017**, *64*(8), 6255–6264.
17. Mather, B.A.; Kromer, M.A.; Casey, L. Advanced photovoltaic inverter functionality verification using 500kw power hardware-in-loop (PHIL) complete system laboratory testing. In Proceedings of the IEEE PES Innovative Smart Grid Technologies (ISGT), Washington DC, USA, February 24–27, **2013**.
18. Faranda, R.; Leva, S.; Maugeri, V. MPPT techniques for PV systems: Energetic and cost comparison. In Proceedings of the 2008 IEEE Power and Energy Society General Meeting – Conversion and Delivery of Electrical Energy in the 21st Century, Pittsburgh, PA, USA, July 20–24, **2008**.
19. Desoto, W.; Klein, S.; Beckman, W. Improvement and validation of a model for photovoltaic array performance. *Sol. Energy* **2006**, *80*(1), 78–88.

20. Kim, D.J.; Kim, B.K.; Ryu, K.S.; Lee, G.S.; Jang, M.S.; Ko, H.S. Development of PV-power-hardware-in-loop simulator with realtime to improve the performance of the distributed PV inverter. *J. Korean Sol. Energy Soc.* **2017**, *37*(3), 47–59.
21. SOLAREX MSX-60 and MSX-64 solar panel datasheet. https://www.solarelectricsu pply.com/media/custom/upload/Solarex-MS X64.pdf